"Gheorghe Asachi" Technical University of Iasi, Romania

REMOVAL OF METHYL ORANGE AND CADMIUM FROM SOLUTION USING MODIFIED ACTIVATED CHARCOAL

Nicoleta Popa[1,2], Maria Visa[1]*

[1]Transilvania University of Brasov, R&D Centre of Renewable Energy Systems and Recycling,
Eroilor 29, 500036 Brasov, Romania
[1,2]Department of Forest District Teliu, National Directorate of Forests Romsilva, Romania

Abstract

In this work, the removal of methyl orange (MO) and Cd^{2+} by simultaneous adsorption on adsorbent obtained from modified charcoal (BCBH) coated with TiO_2 has been studied. The synthesized materials obtained from wood branches were characterized using atomic force microscopy (AFM) for the roughness and SEM to determine the morphology of the surface. EDX spectroscopy indicates the presence of C, N, O, Na, K, P and Ti on the surface of the adsorbent materials. The micro-porosity and BET specific surface were carried out by N_2 adsorption. Additionally, the FT-IR spectroscopy illustrates that hydroxyl, carboxyl groups developed on the adsorbent surface are able to adsorb MO and Cd^{2+}. The effect of the experimental conditions on the adsorption behavior was studied by varying the contact time, amount of adsorbent and initial MO concentration. The adsorption data were modeled using the Langmuir and Freundlich adsorption isotherms equations. The kinetic studies showed that the adsorption followed pseudo-second-order kinetic model. The maximum adsorption capacity (q_{max}) was found to be 5.06 mg/g MO for the adsorbent in hydrothermal activated with NaOH. In case of adsorption from bicomponent systems under mechanical stirring the q_{max} for MO was 5.1 mg/g and for Cd^{2+} cations was 294.11 mg/g for BCBHD1 adsorbent.

Key words: adsorption, cadmium, hydrothermal charcoal, methyl-orange

Received: January, 2019; Revised final: January, 2020; Accepted: January, 2020; Published in final edited form: February, 2020

1. Introduction

The generation and disposal of huge amounts of the industrial waste and other pollutants have heavily contaminated our environment and waters. The synthetic dyes and heavy metals are becoming increasingly prevalent as the most dangerous pollutants in soil and in surface waters. Every year $7*10^5$ tones and over 10,000 different types of dyes and pigments are produced in the World (Kolodynska et al., 2017) and are presented in the effluents of the textile, leather, paper and dye industries. The recent estimates have indicated that, approximately 12% of synthetic textile dyes used each year is lost during manufacturing and processing operation and major amounts of these dyes go in the environment through effluents (Hema and Arivoli, 2007; Pattnaik and Dangayach, 2019). They are causing great concern worldwide due to their toxicity to many life forms. Even if the concentration of the dyes is lower than 1 mg/L this can give undesirable color to water surface. The health effects of the methyl orange are: irritation in case of skin, of eye by contact, of ingestion and of inhalation. Cadmium is a heavy metal and toxic environmental pollutant, classified as a human carcinogen which is mainly coming from electroplating and battery industries.

Many processes have been applied to remove the harmful pollutants, including adsorption (Visa and Duta, 2008; Visa et al., 2011), biosorption (Guerrero-Coronilla et al., 2019; Kumar and Ahmad, 2011; Pholosi et al., 2013), electrochemical coagulation,

---

* Author to whom all correspondence should be addressed: e-mail: maria.visa@unitbv.ro; Phone: +40-729109355

photodegradation (Matos et al., 2017), membrane filtration (Yang and Garrahan, 2005), electro flocculation and ozonation (Ciardelli and Ranieri, 2001), photo-Fenton (Visa and Duta, 2013), and simultaneous methods (Visa and Nacu, 2011). The adsorption method is intensely used for removing soluble and insoluble pollutants from surface water and from wastewater without the generation of hazardous by-products (Popa and Visa, 2017) being inexpensive, with simple equipment, easy to operate and with highly effective treatment.

The adsorbents materials produced from biomass of the forest, agricultural by-products have been used, such as: raw wood (Yagmur et al., 2013), pine biomass (Ofomaja et al., 2015), waste from grape industrial processing (Sayğili et al., 2015), wheat straw (Robinson et al., 2002; Zhang et al., 2014;), rice husk (Chakraborty et al., 2011), orange peel (Sivaraj et al., 2001), oak leaves, palm leafs (El-Shafey et al., 2016), Korean cabbage waste (Sewu et al., 2017). The biocharcoal obtained from them follows to be chemical or physical activated. Environmentally friendly utilization of agricultural by-products/waste materials for removal the pollutants from the wastewater is an opportunity to solve a waste by other waste. The preparation of the charcoal from tree branches (forest waste/biomass) using the built "Bocsa" may appear a valuable path. Because, its burning is slow, takes approximately 2-3 weeks, depending on the size of the Bocsa. The oxygen intake is controlled therefore; combustion should be slow which may offer a good carbonization of this biomass.

The aim of this work is to obtain the mesoporous charcoal by hydrothermal method modified in alkali environmental and impregnated with TiO$_2$ (Degussa P25), used as an adsorbent for simultaneous removal of methyl orange (MO) dye and cadmium cations (Cd^{2+}) from aqueous solution.

2. Experimental

2.1. Preparation of materials and substrate

The precursor material was the tree branches collected from deciduous forest of Brasov, Romania. The branches were carbonized with an insufficient amount of air up to 400-550 °C and then the channel was blocked and left few days to cool. The process of obtaining biocharcoal (BC) from wood waste can be divided into three steps:

1. Drying: in this phase water is eliminated from branches, virtually drying occurs between 0-110°C;

2. Dry distillation: occurs between 150- 350°C. At 180°C hemicelluloses and 1/3 of cellulose usually begin decomposition, and the wood resistance drops significantly when the temperature reaches 260°C;

3. Charcoal formation: the beginning of this stage is at 350 - 400°C, ending at 400 - 550°C, depending on the production conditions. This stage is characterized by removing large amounts of incondensable gases resulting from breakdown of cellulose and lignin (Li et al., 2001; Suhas et al., 2016; Yang et al., 2007). This

biocharcoal was activated with NaOH in hydrothermal conditions, at 100 °C, stirred 24 h and, then was washed with ultra-distillate water and dried at 105 - 115°C till constant mass. This adsorbent material was noted (BCBH).

2.2. Modification of BCBH with TiO$_2$

To improve the adsorbent and photocatalytic properties of the BCBH substrate, three composites noted as BCBHD1, BCBHD2 and BCBHD3 were developed by adding the TiO$_2$ (Degussa P25, 80% anatase and 20% rutile) to BCBH substrate in ratio 1:1; 1:2; 1:3 under ultrasounds for 10 h.

These composites were tested as adsorbents for removal of the MO and Cd^{2+} cations from aqueous solution. It is expected that, due to the synergistic effect of the exposed functional groups (-OH) and TiO$_2$ on the charcoal surface, the new composites will exhibit a good adsorption and photocatalytic ability in the wastewater treatment process.

2.3. Materials characterization

The surface morphology of the substrates was observed using Scanning Electron Microscopy (SEM, model S-3400N-Hitachi) at 20 -30 kV. The surface elemental composition was evaluated using Energy Dispersive X-ray (EDX) measurements. The surface roughness and macro-pores size distribution was evaluated using AFM (Ntegra Spectra, NT-MDT model BL222RNTE). The FT-IR spectra of the samples were recorded with Spectrum BX Perkin Elmer BX II 75548, λ=400 – 4000 nm to analyze the surface functional groups. The XRD patterns of the samples were recorded using an X-ray diffractometer (XRD Bruker D8 Discover Diffractometer) operating at 40 kW and 20 mA, 2θ range from 10 -70° and scan speed 2s/step).

2.4. Adsorption experiments

2.4.1. Experimental conditions

The pollutant systems were synthetically prepared using ultrapure water with resistivity of 18.23 MΩ cm^{-1}, CdCl$_2$·2.5H$_2$O (Scharlau Chemie S.A., c<98 %) and MO(C$_{14}$H$_{14}$N$_3$NaO$_3$S) (Fluka AG., with molecular weight (327.33 g/mol). The experiments were done using solutions in the concentrations of C$_{Cd}$= 0.01 N, C$_{MO}$= 0.03125 mM. A series of the experiments on adsorption were done: - adsorption under mechanical stirring with: (a) MO and (b) MO+Cd^{2+} on BCBH, BCBHD1, BCBHD2 and BCBHD3. In order to demonstrate the adsorbent capacity of the adsorbents, the methodology followed the steps below: adsorption parameters determination - *contact time* (t), *ratio of solution volume, adsorbent dose (V$_{sol}$/m$_s$), initial concentration of pollutants;* kinetic models investigation - pseudo-first-order, pseudo second-order, intra particle diffusion, to establish the adsorption mechanisms; the adsorption isotherms Langmuir and Freundlich were investigated.

2.4.2. Effect of contact time and adsorbent dose on adsorption efficiency

In order to optimize the contact time, 0.1 g of the adsorbent at the temperature range 20 - 23 °C, were dispersed in MO and MO+Cd^{2+} solutions with C$_{MO}$= 0.03125 mM and C$_{Cd}$=0.01N, initial concentration. The suspension was stirred at 100 rpm. for 10, 20, 30, 45, 60, 90, 120, 150, 180 min, then the substrate was removed by filtration on 0.45 μm filter. After adsorption, the residual dye concentration (MO) in supernatant solution was analyzed by UV-VIS spectrometry (Perkin Elmer Lambda 25) on the calibration curve registered at the maximum absorption peak of MO (λ=464nm). The Cd^{2+} cations concentration was analyzed by AAS (Analytic Jena, ZEEnit 700) at λ$_{Cd}$ = 228.8 nm. The losses due to adsorption onto the flask walls and filter paper were negligible. The removal efficiency of the pollutants, [%], were calculated by Eq. (1):

$$\eta = (c_0 - c_t) * 100 / c_0 \ [\%] \qquad (1)$$

where: c_0 is the initial concentration (mg/L); c_t is the concentration at moment t (min).

The amount of MO or Cd^{2+} cations adsorbed at any time, q_t (mg.g^{-1}), was calculated by Eq. (2):

$$q_t = (c_0 - c_t) \times V_{sol} / m_s \qquad (2)$$

The results of pollutants, MO and Cd^{2+} removal from solutions on substrates are presented in Fig. 1.

Fig. 1 shows a rapid adsorption of MO dye at the initial stages of the adsorption and the equilibrium was attained within 30-45 min. The adsorption efficiency of the MO on each substrate in present of cadmium cations is higher with 10-20 % than in absences of Cd^{2+} cations. Such uptake indicates a high degree of affinity towards the MO molecules via chemisorption or more active sites are developed in present of TiO$_2$.

The best performance was obtained for substrates BCBHD1 and BCBHD2, which showed adsorption of Cd^{2+} cations than 69.62 % and 60.42 % respectively at 60 min. comparing with 13.82 % of the BCBHD3. In this case a higher amount of TiO$_2$ added to charcoal would favor photocatalyst over adsorption.

At optimal contact time, 45 min, the percentages removal of MO and of the Cd^{2+} cations increased with the increase in dose of the adsorbent (Fig. 2). This may be due to the increase in availability of surface-active sites resulting from increased dose and conglomeration of the adsorbent particles.
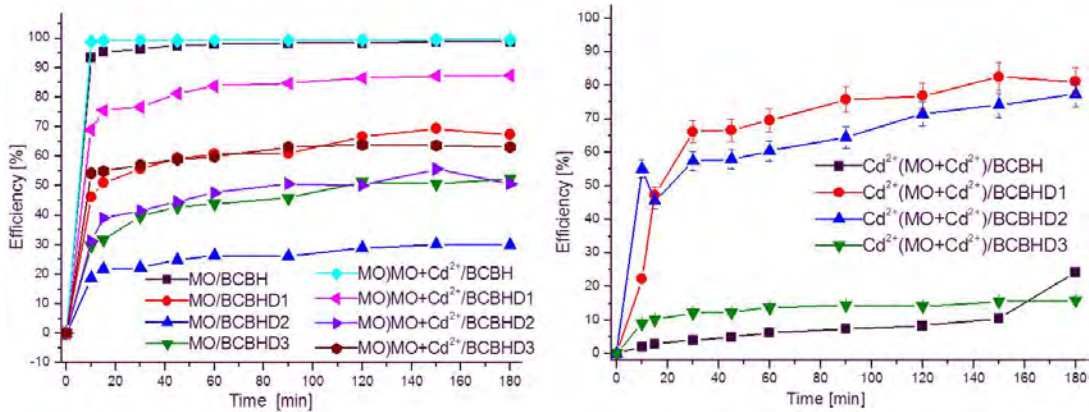
Fig. 1. Removal efficiency vs. time of MO dye, MO dye in present of Cd^{2+} cations; and of Cd^{2+} cations from di-solute aqueous solutions
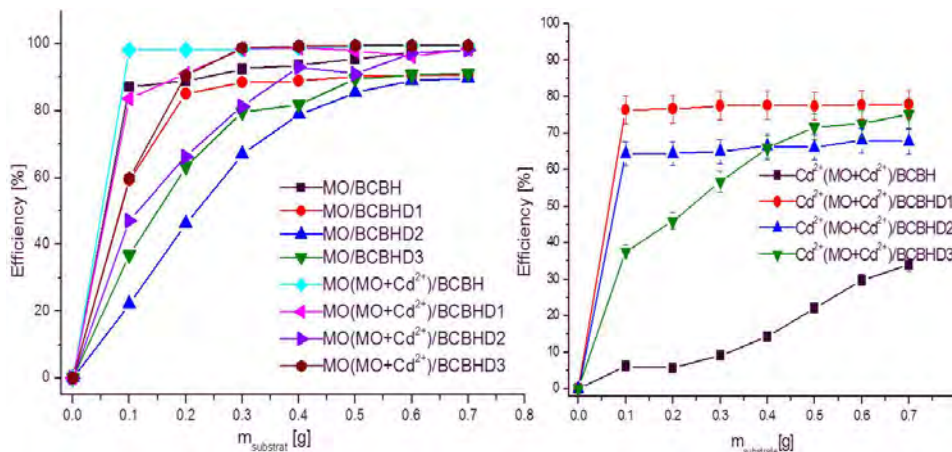
Fig. 2. Adsorption efficiency of MO and of Cd^{2+} cations on different amounts of adsorbent

As it can be seen in Fig. 3.b, at the equal concentrations, q_t adsorbate/g adsorbent changed the hierarchy of adsorbed species, while that of adsorbent maintain the same trend. This aspect shows that a higher number of Cd^{2+} cations are adsorbed by comparing to the number of MO dye, due to the dimensional reasons.

3. Results and discussions

3.1. Crystalline structure of substrate

The phase's composition of BCBH, BCBHD1, BCBHD2 and BCBHD3 were evaluated with XRD analysis and the XRD patterns are presents in Fig. 4.

The modified charcoal (BCBHD1; BCBHD2; BCBHD3) composition is confirmed by the XRD analysis and the results are presented in Table 1. The predominant crystalline components of BCBH are: (SiO_2), Nitratine, syn$(NaNO_3)$ and $Mg_3Fe_2(SO_3)6H_2O$ while anatase and rutile are prevalence in substrates BCBHD1, BCBHD2 and BCBHD3. The XRD data show that the new modified biocharcoal has well embedded titanium oxide with crystallite sizes from 145 to 277.8 Å. The crystallites size, τ, was calculated using the Scherrer relationship (Eq. 3).

$$\tau = K\lambda / \beta \cos\theta \qquad (3)$$

where: K is the shape factor with a typical value 0.94; λ is the X-ray wavelength (1.541 Å); β-is the line broadening at half the maximum intensity (of a peak); θ- is the diffraction angle.

Also, traces of K, Na and P species were identified as impurities of the BCBHD substrate.
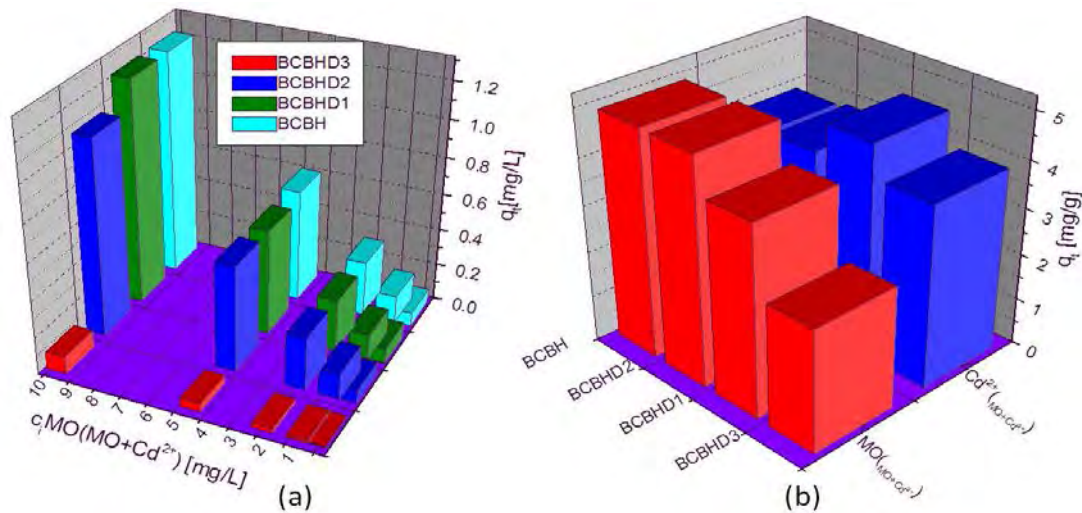
Fig. 3. Adsorption capacity (a); at different concentrations; (b) for MO and Cd^{2+} cations at the equal concentrations (10 mg/L)
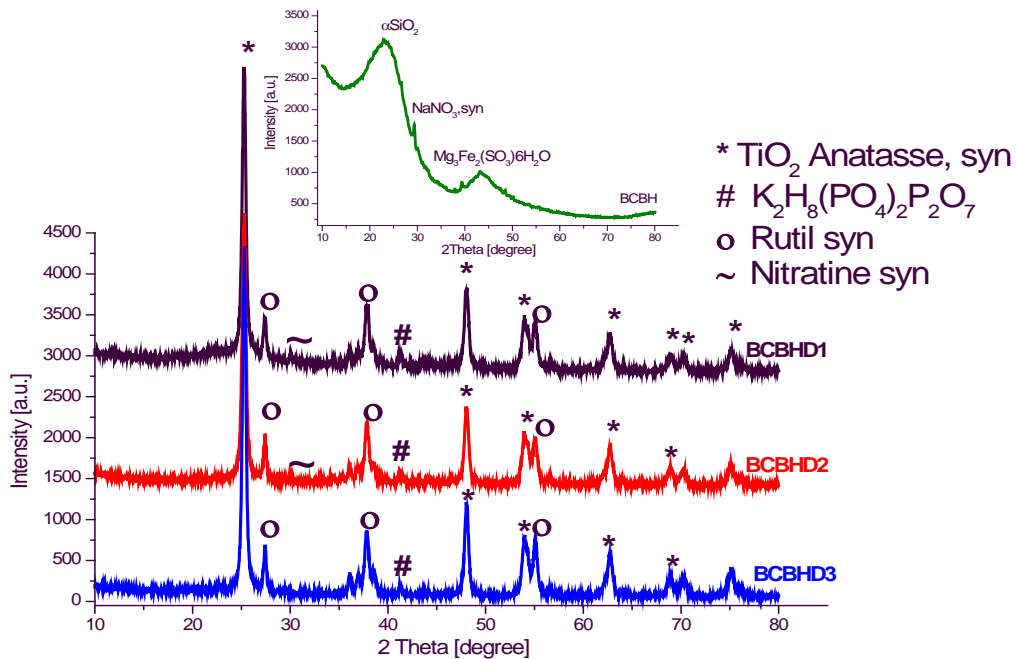
Fig. 4. XRD patterns of the samples: (a) BCBH; (b) BCBHD1; BCBHD2; BCBHD3

Table 1. The composition of the crystalline phases

2θ	COD/PDF	Crystalline phases	Structures of the crystallite	Crystallite size (Å)	Crystallinity [%]
			BCBH		
23.26	00-028-0790	αSiO$_2$ Silicon Oxide	triclinic	343.2	
29.36	00-022-0841	Na(NO$_3$) Nitratine, syn	rombo.H.axe	426.6	51.60
43.36	01-088-0537	Mg$_3$Fe$_2$(SO$_3$)6(H$_2$O)	triclinic	271.6	
			BCBHD		
25.309	00-064-0863	TiO$_2$ Anatase, nano	tetragonal	211.7	
29.383	01-070-1518	NaNO$_3$ Nitratine, syn	rhombo.H	604.2	BCBHD1
36.996	00-064-0863	TiO$_2$ Anatase, nano	tetragonal	212.9	73.6
48.032	00-004-0477	TiO$_2$ Anatase, syn	tetragonal	184.9	
53.985	00-064-0863	TiO$_2$ Anatase, nano	tetragonal	145	BCBHD2:
62.739	00-064-0863	TiO$_2$ Anatase, nano	tetragonal	165.5	90.9
56.683	00-004-0478	TiO$_2$ Rutile	monoclinic	252.3	
	00-025-0638	TiO$_2$ Rutile	monoclinic	276.1	BCBHD3:
41.207	00-021-0385	K$_2$H$_8$(PO$_4$)$_2$P$_2$O$_7$	orthorhombic	277.8	81.6

3.2. Morphology and surface tension of the substrates

The AFM images (Figs. 5a, b, c) and pore size distributions (Fig. 5d) show the different granular shape in the size range of 0 -200 nm, also give information about the distribution of TiO$_2$ on charcoal that is very important in adsorption process.

The AFM images give information about the rough surface with larger pores/voids heterogeneously distributed that is confirmed by the pores/voids distribution curve in Fig. 5 (d). Thus, low roughness value (9.621 nm; 11.332 nm) of the BCBHD2 and BCBHD3 displays a higher number of aggregates differently in shaped (almost round) and stable.

(a) Average roughness:173.927nm

(b) Average roughness: 9.621 nm

(c) Average roughness:11.332 nm

(d)
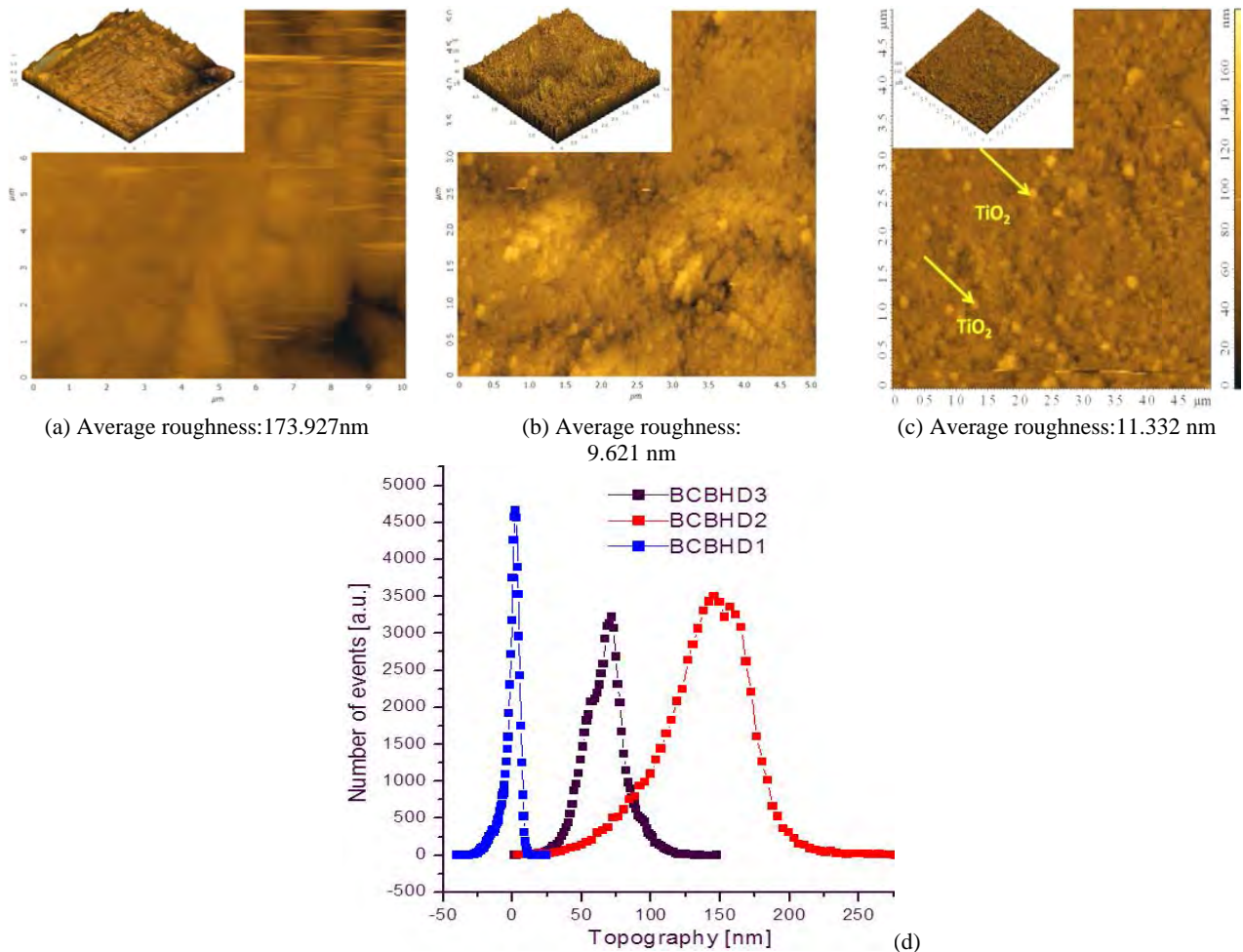
Fig. 5. The AFM topography (a) BCBHD1 (b) BCBHD2, (c) BCBHD3; (d) Pore histogram

The porosity parameters of these adsorbents such as S_{BET}, pore volume and micropores volume are presented in Table 2. The surface increases after hydrothermal treatment with NaOH and decreases by adding TiO_2 with S_{BET} of 50 m²/g.

Table 2. The S_{BET} and pores structures

Sample	S_{BET} [m²/g]	V_t [cm³/g]	$V_{micro\ pores}$ [cm³/g]
BCBH	387.882	0.217	0.126
BCBHD1	241.388	0.271	0.062
BCBHD2	128.405	0.243	0.049
BCBHD3	74.267	0.228	0.018

The morphology/topography of the substrates was obtained from the SEM micrographs (Fig. 6a). The SEM images of the surface and the surface composition of the hydrothermal charcoal (BCBH) and of BCBHD with Degussa P25 are shown in Figs. 6a, a`, b, b`, c, c`, d, d`. Many honeycomb- shape gaps with diameters over 4.0 µm appear on the surface of BCBH. These irregular gaps are surrounded by contracted twisted walls. The walls are thick and smooth without any structure. Based on the SEM images, when the charcoal particles are in contact with NaOH, a thin film of NaOH should cover their surface and the interior of chars should be covered with Na^+

and HO^- that are displayed in XRD spectra. However, the watering of NaOH to the gap interior favors the micropore development that results in an increase of the micropore number (Ho et al., 2000; Tseng and Tseng, 2005). The cavities are very irregular indicating that, during activation, the alkaline reagent (NaOH) caused a higher porosity in the adsorbent materials. The high density of the precursor has an importance contribution to enhance of amount of the carbon from 52.47 to 100 wt.% in BCBH or from 15.12 to 100 wt.% in substrates with TiO_2, respectively.

The SEM images confirm that the charcoal particles were cracked and micro-restructuring occurred with significant modification of the surface aspect, as results of/imbedded of nano-sized TiO_2 in the micro BCBH grains. The hydrothermal process promotes the surface interactions, including dissolution, re-crystallization, re-precipitation of the charcoal raw components and new components are developed.

From SEM, AFM and BET isotherm resulted that MBCBH is characterized by the high porosity, high BET surface, high micro-pores volume, and all these explain the best adsorptive capacity of the BCBH substrate. The titanium oxide added at BCBH substrate favors the adsorption of Cd^{2+} or another species of cadmium which exist in system.

(a)

(b)

(c)

(d)

C:52.47-100Wt.%
N:52-100wt%
and:
O; Na; Al; Si.

(a`)

C:32.47-100Wt.%
N:52–75wt%
Ti:16.8– 98.2wt%
and:
O; Na; Al; Si.

(b`)

C:30.25-100Wt.%
N:52-100wt% Ti:22.4–
100Wt%
and:
O; Na; Al; Si

(c`)

C:15.12-100Wt.%
N:32-53.3wt%
Ti:70.4–100Wt%
and:
O; Na; Al; Si.
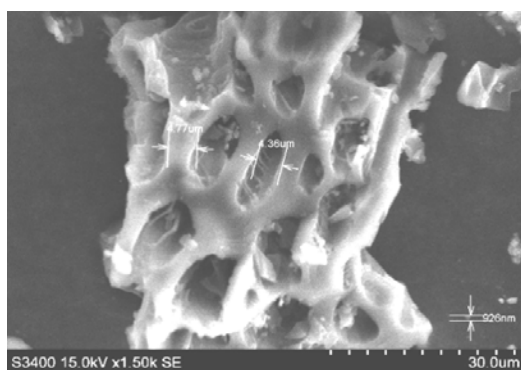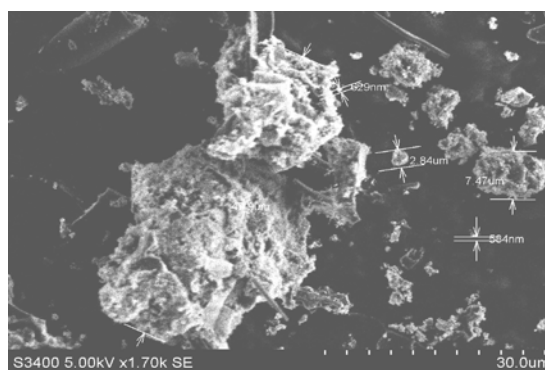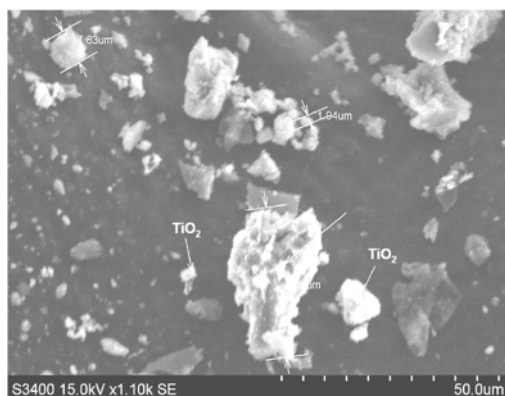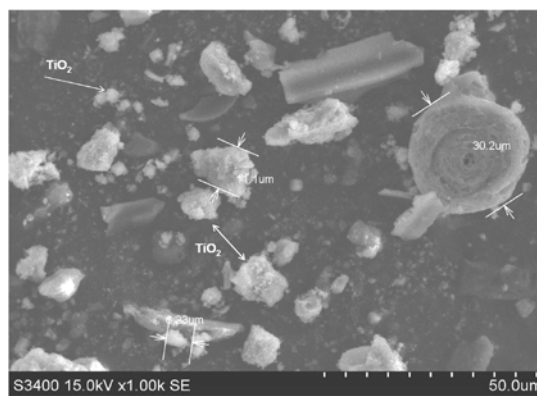
(d`)
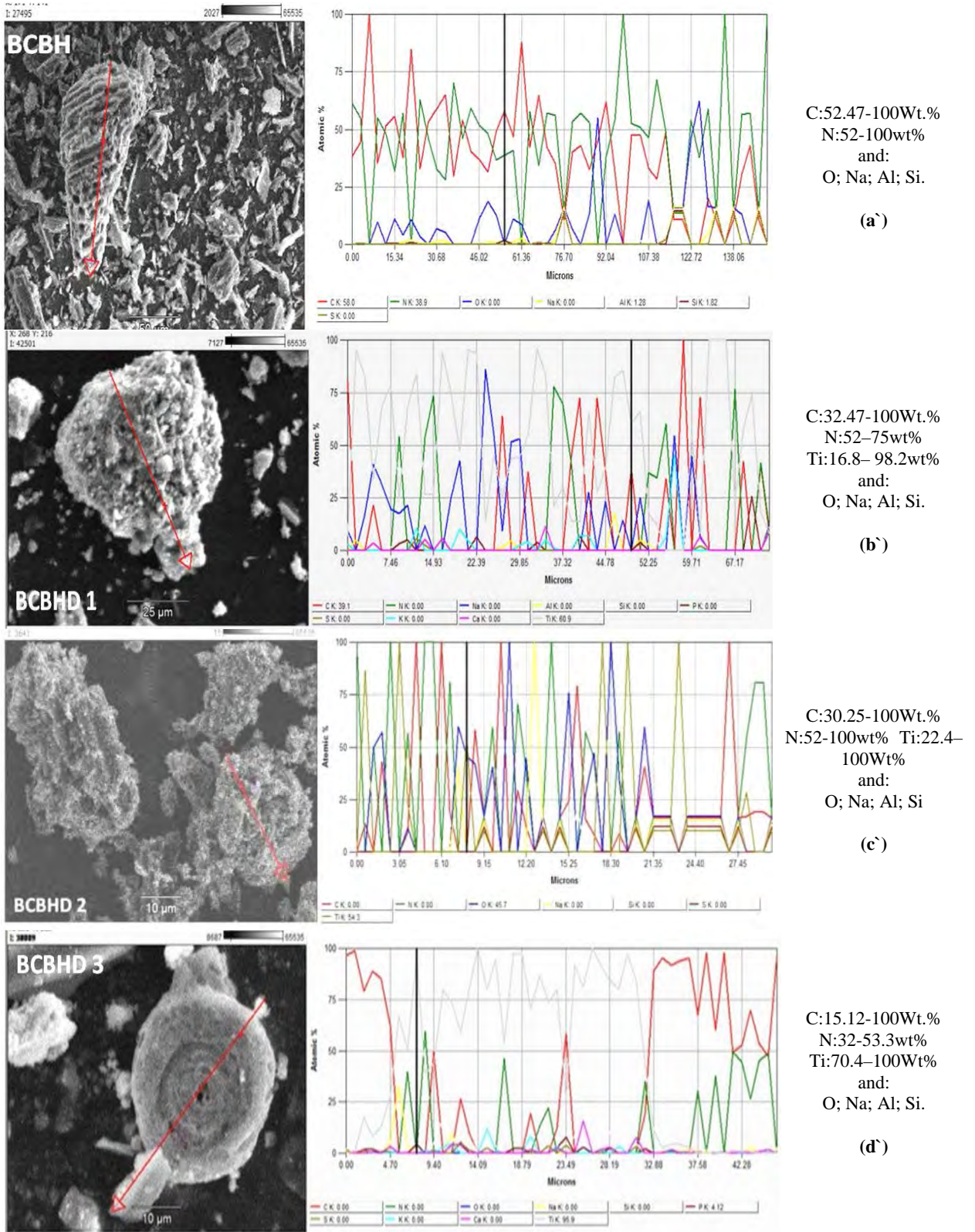
Fig. 6. (a) SEM micrographs of BCBH; (b) SEM micrographs of BCBHD1; (c) SEM micrographs of BCBHD2; (d) SEM micrographs of BCBHD3; (a`) EDX image of BCBH on the agglomerate; (b`), (c`), (d`) EDX images of BCBHD1, BCBHD2, BCBHD3 on the agglomerate with TiO_2

3.3. FT-IR analysis of the adsorbent substrates

The infrared spectrum of the adsorbent materials BCBHD1, BCBHD2 and BCBHD3 was performed to identify chemical bounds as well as functional groups. Each sample was scanned from 400 to 4000 cm^{-1} and the peaks were examined (Fig.7). Strong absorption in the frequency region of 410-1000 cm^{-1} corresponds to Ti–O–Ti bonding. The mixture of polymorphic phases of anatase and rutile was

observed from 400–820 cm^{-1} in the composites. The absorption peaks at 595 and 600 cm^{-1} shows the rutile phase on surface of the composites. The characteristic peaks at 1450 and 1630 cm^{-1} revealed the existence of ketone or aldehydes carbonyl stretching, while latter conjugated with aromatic rings. The peaks around 2355cm^{-1} were assigned to the asymmetric or symmetric deformation of C–H in methyl and methylene (Li et al., 2001; Yang et al., 2007)

Adsorption as surface process is influenced not only on the crystallinity and morphology, but also by surface charge. Surface charge depends on the pH of the solution and must be discussed based on the value(s) of the point of zero charge (PZC). The pH $_{PZC}$ of BCBH and BCBHD substrates depends on the alkali-acid character of surface hydroxyl, carboxyl lactone groups.

The pH in the aqueous solution is lower than pH$_{PZC}$, the surface is positively charged, and when pH in the aqueous solution is higher than pH$_{PZC}$, the surface is negatively charged. The calculated pH$_{PZC}$ for BCBH, BCBHD1, BCBHD2 and BCBHD3 are from 7.77 to 8.96, 9.67, 9.97 that explains well the high adsorption efficiency of MO and of cadmium on new substrates. The working pH is over 7.8 value and as results the adsorbent surface is negative and Cd^{2+} cations and other hydrated species or precipitate can be adsorbed.

4. Adsorption kinetics modeling

The kinetic data of the adsorption studies were processed to understand the adsorption mechanism of the MO on substrates with TiO$_2$ embedded onto hydrothermal charcoal and the adsorption mechanism of MO with Cd^{2+} cations. In the present study, the applicability of the pseudo-first-order (Eq.4), pseudo-second-order and intraparticle diffusion models (Eqs. 5, 6 and 7) were tested. These models have been fitted with experimental data at various physico-chemical conditions for which all fitting plots are not presented here. The plot t/qt versus t, should give a straight line with higher linear correlation coefficients if pseudo-second-order kinetics is applicable, and qe, k$_2$ can be determined from the slope and intercept, Fig. 8.

The pseudo-first order equation of Lagergren is generally expressed as follows (Mahmood et al., 2017) Eq. (4)

$$log(q_e - q_t) = log(q_e) - K_L t / 2.303 \qquad (4)$$

where: K_L (min^{-1}) is the Lagergren constant (the adsorption rate constant); q_t and respectively q_e (mg·g^{-1}) are the amount of adsorbed pollutants by adsorbent at time t (min) and respectively at the equilibrium.

The second kinetic model applied was the pseudo-second order. The rate expression is based on the adsorption capacity of the solid phases, which has been investigated using the kinetics of the chemisorption processes. It is calculated by means of the equation developed by Ho and Mc Kay, Eq. (5), (Ho and Mc-Kay, 1998; Mahmoud et al., 2016;).

$$t / q_t = 1 / k_2 q_e^2 + t / q_e \qquad (5)$$

where: k_2 is the equilibrium rate constant for the pseudo-second order adsorption (g mg^{-1} min^{-1}). The adsorption capacity at equilibrium *(q$_e$)* and adsorption rate constant *(k$_2$)* are determined from the slope and intercept of linear plot of *t/q$_t$* against *t* for Eq. (5) This model is based on the assumption that the rate limiting step may be a chemisorption involving the valence forces through sharing or exchange of electrons between the adsorbent and the adsorbate (Duman et al., 2009). The pseudo-second order kinetic (Eq. 5) is the model which best describes the adsorption of the pollutants on the new adsorbent materials.
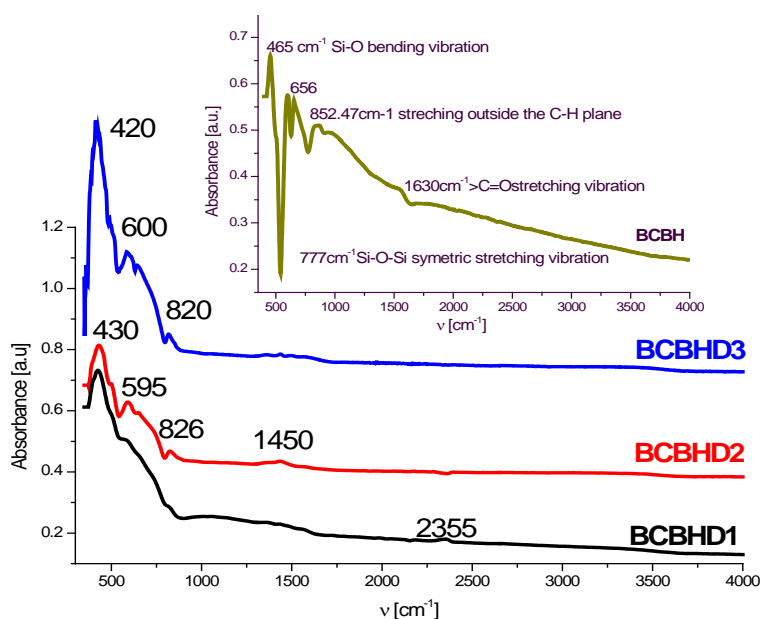
Fig. 7. FT-IR spectrum of substrates

Intra-particle diffusion model developed by Weber and Morriss is used to identify the rate controlling step in the adsorption process and the mechanism of adsorption. The mechanism of adsorption involves multiple steps: the MO molecules or Cd^{2+} cations migrant from the bulk solution to the surface of the adsorbent diffuse through the boundary layer to the surface of adsorbent and followed by intra-particle diffusion into the interior of the adsorbent. The amount of MO or Cd^{2+} cations can be calculated by Eq. (6).

$$q_t = K_{id}t^{1/2} + C \qquad (6)$$

where: k_{id} is the intra-particle diffusion rate constant $(mg·g^{-1}·min^{-0.5})$ and it can be calculated from the slope of the linear Eq. (6) of the linear plot q_t against $t^{1/2}$. The constant C $(mg·g^{-1})$ indicates the thickness of the boundary layer. Higher C values are indicative of higher boundary layer effect and thus are descriptive of the inapplicability of pore diffusion as the sole rate-determining step in describing the dynamics of the adsorption process (Alijeboree et al., 2017). The kinetic parameters are presented in Table 3. A linear relationship between t/q_t against t and almost identical values between q_e and q_t indicate the applicability of this model. The linearization proved that the pseudo-second kinetic order describes fairly well the adsorption mechanism for MO and for the Cd^{2+} cations in all cases (Fig. 8).

The correlation coefficient of the second order kinetic model (1) is greater than for the first order kinetic model (0.906), while the MO adsorption on BCBH proved also to be faster $(k_2= 0.1115$ g $mg^{-1}min^{-1})$ as $(k_1=0.0223$ $min^{-1})$. This confirms that the rate limiting step is chemisorption (Hsu et al., 2011).

Kinetic experiments clearly indicated that adsorption of methyl orange on substrate obtained from wood biomass is a two-step process: a rapid adsorption of dye onto the external surface followed by intra-particle diffusion into the interior of adsorbent which has also been confirmed by intra-particle diffusion model.

5. Adsorption isotherms modeling

At contact time optimal by 45 min, determined from the adsorption efficiency in time (Fig. 1 and Fig. 2) and m_{ss}/V_{sol} ratio (0.2 g/50 mL for adsorption of MO), the adsorption isotherms were ploted at different MO concentration (10.228-0.639 mg/L). Based on optimised parameters, the adsorption isotherm q = f(Ce) was plotted.

The adsorption isotherm models investigated were based on Langmuir and Freundlich equations, Eqs. (7, 8) and (9):
- *the Langmuir isotherm (linear form):*

$$C_{eq} / q_{eq} = 1/ q_{max}K_a + C_{eq} / q_{max} \qquad (7)$$

where: q_{max} represents the maximum monolayer adsorption capacity (mg g^{-1}); K_a is Langmuir constant (L mg^{-1}) related to the adsorption free energy, q_{eq} is the amount of dye adsorbed from the solution at the equilibrium time; C_{eq} is equilibrium concentration of dye in solution ((mg g^{-1}). From the slop and intercept of the plot between C_{eq}/q_{eq} vs. C_{eq} the values of K_a and q_{max} respectively, are calculated. The isotherm model was expressed in terms of the dimensionless constant separation factor R_L, Eq. (8).

$$R_L = 1/1 + K_a C_0 \qquad (8)$$

where: C_0 is the initial dye concentration (mg g^{-1}); R_L- the separation factor and can be determined from Langmuir plot with the Eq. (7) and indicates the type of adsorption. For the values of $R_L= 0$ adsorption can be irreversible, for $0.00<R_L<1$, adsorption is favorable, for $R_L =1$ the adsorption is linear, while $R_L >1$ is the indicative of unfavorable adsorption (Bhatti et al., 2017).

Table 3. Kinetic parameters of the adsorption processes

Adsorbent	Pseudo-first order			Pseudo-second order			Intra-particle diffusion		
	K_L (min^{-1})	$q_{e(exp)}$ (mg/g)	R^2	k_2(g/mg·min)	$q_{e(cal)}$ (mg/g)	R^2	K_{id} (mg/g min$^{0.5}$)	C (mg/g)	R^2
MO from monopollutant system									
BCBH	0.0223	5.059	0.906	0.1115	5.066	1.00	0.017	4.845	0.842
BCBHD1	0.0161	3.547	0.907	2.1439	3.605	0.997	0.103	2.215	0.918
BCBHD2	0.0226	1.539	0.908	5.004	1.574	0.995	0.054	0.862	0.938
BCBHD3	0.0205	2.688	0.905	4.3152	2.831	0.997	0.111	1.306	0.929
MO from (MO+Cd^{2+}) system									
BCBH	0.0154	5.092	0.821	0.0161	5.092	1.00	0.001	5.078	0.821
BCBHD1	-	4.466	0.461	0.6587	4.490	0.997	0.064	3.515	0.516
BCBHD2	0.0089	28.00	0.981	2.1882	2.755	0.994	2.444	8.56	0.952
BCBHD3	0.0239	3.225	0.961	0.8115	3.304	0.999	0.051	2.642	0.945
Cd^{2+} from (MO+Cd^{2+}) system									
BCBH	0.0032	29.00	0.983	1.82	38.61	0.938	1.959	2.4	0.997
BCBHD1	0.0193	237.5	0.870	0.070	294.12	0.991	8.929	125.5	0.849
BCBHD2	0.0145	222.6	0.929	0.044	227.27	0.989	7.655	118.1	0.901
BCBHD3	0.01727	45.35	0.892	0.187	46.083	0.994	1.751	23.03	0.919
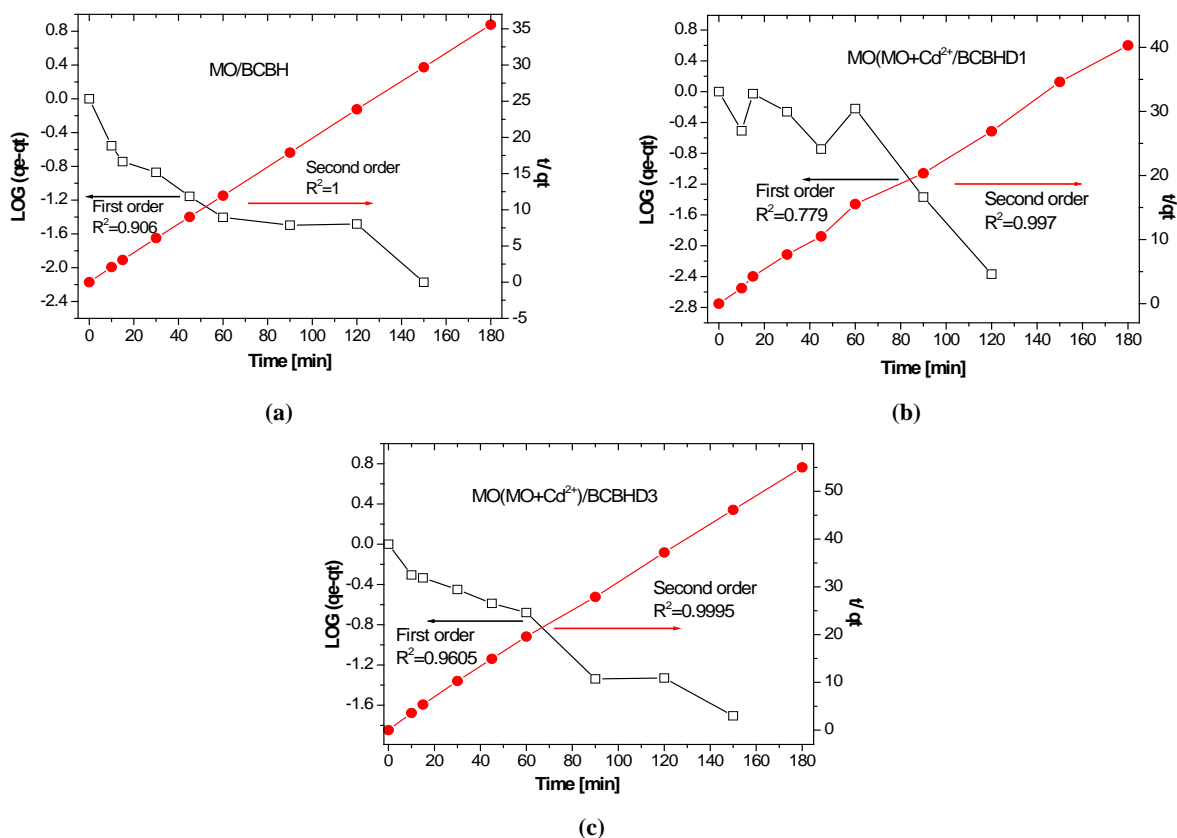
Fig. 8. The pseudo first order and the second order kinetic plot for MO adsorption on BCBH (a), BCBHD1 (b) and BCBHD3 (c)

- *the Freundlich isotherm (linear form):*

$$ln\, q_{eq} = ln\, k_F + 1/n\, ln\, c_{eq} \qquad (9)$$

where: k_F is Freundlich constant indicating the adsorption capacity; $1/n$ is a dimensionless parameter indicating the adsorption density.

The parameters of both models are presented in Table 4 and outline that chemisorption is as described by the Langmuir model. The results show a significantly higher adsorption capacity of the substrate during adsorption. Generally, the value of the linear regression correlation coefficient R^2 gives the indication which model to choose to give best-fit. The values of R^2 (0.998; 0.946) and q_{max} = 6.165 mg/g; 2.926 mg/g indicate that the Langmuir adsorption model can well discribe the removal of the MO by using BCBH adsorbent, and BCBHD3, respectively. For the values of R_L (0.00<R_L<1), adsorption can be favorable. The Freundlich adsorption isotherm model yields a heterogeneous adsorption surface with unequal available sites and different adsorption energies. All the substrates on methyl orange adsorption also can be described by Freundlich isotherm (R^2 = 0.990; 0.979; 0. 950). The value of $1/n$ closer zero (0.565 -1.245) indicates more surface heterogeneity on certain areas. The adsorption of Cd^{2+} cations is fitted on Langmuir model isotherm on BCBH, BCBHD1 and BCBHD3 with q_{max} = 45.456 mg/g. Generally, the best isotherm model is chosen based on a high linear regression coefficient (R^2) value. Table 5 show a comparison with the maximum adsorption capacities of several adsorbents found in literature. The results obtained in this work are in same order of magnitude as the reported materials.

Two parallel adsorption mechanisms occurs, one involving electrostatic interactions and a second one involving dispersive interactions. In aqueous solutions at pH> pH$_{PZC}$ the present of TiO$_2$ may have a positive effect in adsorption of Cd^{2+} cations, according to the Eqs. (10, 11), (Janusz and Matysek, 2006; Visa and Duta, 2013).

$$\equiv\equiv Ti–OH + HO^- \rightarrow \equiv\equiv Ti–O^- +H_2O \qquad (10)$$

$$2\equiv\equiv Ti–O^- +Cd^{2+} \rightarrow (\equiv\equiv Ti–O^-)_2 Cd^{2+} electrostatic\ interaction \qquad (11)$$
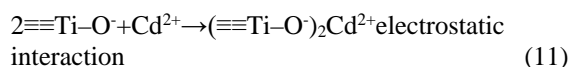
The charcoal (BCBH) is adsorbent with acidic and basic groups (- COOH; - HO) that can interact with Cd^{2+} cations (Pyrzynska, 2019).

6. Regeneration and reuse of the adsorbent

Moreover, the subsequent regeneration and reuse of the adsorbent are important attributes of the adsorption process from economic and environmental viewpoint. In this paper, the reusability of BCBHD3 adsorbent is presented. This adsorbent loaded with MO and cadmium was regenerated using absolute ethanol, bidistilated water and drying at 115 ^{0}C. The adsorption studies were done in the same conditions that in the first cycle: 0.1 g BCBHD3 regenerated, $C_{0/MO}$ = 0.03125 mM, $C_{0/Cd}$ =0.01 N. The results are presented in Fig. 9.

Table 4. Adsorption isotherm parameters for MO and Cd^{2+} removal on adsorbents

Adsorbent	Langmuir Isotherm				Freundlich Isotherm		
	q_{max} [mg g^{-1}]	K_a [L mg^{-1}]	R^2	R_L	n	K_F	R^2
MO from monopollutant system							
BCBH	6.165	0.0383	0.823	0.7186	0.803	0.3334	0.998
BCBHD1	-	-	0.408	-	0.933	0.1258	0.994
BCBHD2	1.423	0.6088	0.903	0.1382	1.590	1.2E-05	0.969
BCBHD3	2.926	0.0996	0.946	0.4952	1.767	2.2E-12	0.979
MO from (MO+Cd^{2+}) system							
BCBH	-	-	0.055	-	0.878	0.0036	0.948
BCBHD1	-	-	0.349	-	0.763	0.0051	0.932
BCBHD2	2.238	0.3471	0.873	0.2196	1.200	1.5E-11	0.970
BCBHD3	-	-	0.776	-	-	3.5E-09	0.805
Cd^{2+} from (MO+Cd^{2+}) system							
BCBH	9.823	0.0930	0.995	0.0191	1.934	0.0022	0.950
BCBHD1	43.49	0.004	0.975	0.3051	3.648	1.5381	0.713
BCBHD2	-	-	0.049	-	1.052	0.9E-08	0.938
BCBHD3	45.46	0.0138	0.963	0.6396	-	-	0.475

Table 5. Comparative adsorption capacities of Cd $^{2+}$ cations and of MO on different adsorbents (Pyrzynska, 2019)

Adsorbent	$Q_{max/Cd}$ [mg/g]	$Q_{max/MO}$ [mg/g]	References
Alginate–calcium carbonate	10.20	-	(Mahmood et al., 2017)
Chitosan-AC	52.63	-	(Hydari et al., 2012)
Na-magadiite	57.00	-	(Attara et al., 2018)
Chitosan derivative	98.04	-	(Boamah et al., 2015)
Apple peels	0.80	-	(Abdolali et al., 2016)
Mandarin peels	3.33	-	
Coffee grounds	16.20	-	(Dutta et al., 2015)
Orange peel	40.00		(Gupta and Nayak, 2012)
Orange peeland Fe2O3 nanoparticles	76.02	-	
Orange peel modified with KCl	125.60	-	(Liu et al., 2010)
Banana peels	5.91	-	(Deshmukh et al., 2017)
Sun flower plant	35.97	-	(Pyrzynska K, 2019)
Aguaje stones	26.33	-	(Hydari et al., 2012)
Camel Thorn Plant	-	19.61	(Mogaddasi et al., 2010)
Moringa peregrine	-	15.43	(Bazrafshan et al., 2014)
BCBH	9.82	6.16	This study
BCBHD1	43.49	4.49	This study
BCBHD3	45.35	3.22	This study
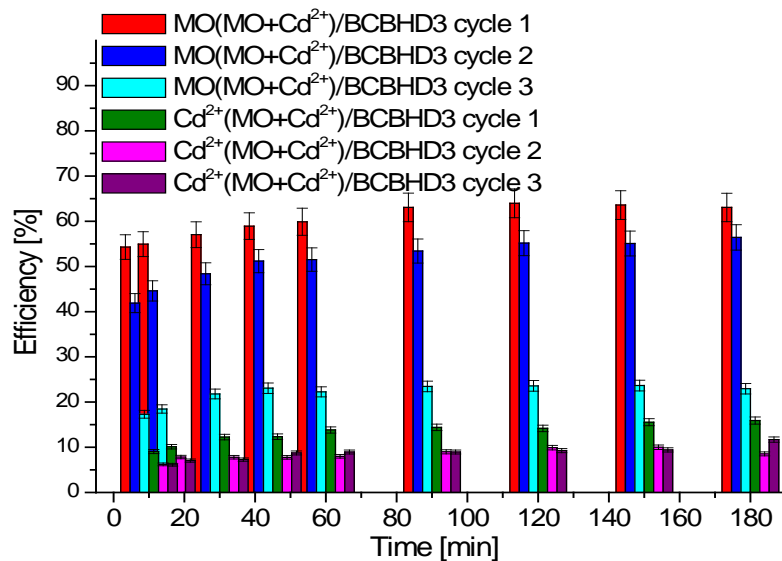
Fig. 9. Efficiency simultaneous removal of MO and Cd^{2+} cations from aqueous solutions by reusing the BCBHD3 adsorbent

The adsorption efficiency of reusability of BCBHD3 adsorbent decreased with increasing desorption cycles. Almost with 15.62 % decreased the adsorption efficiency of MO in the second cycle and with 56.20 % in the third cycle. Adsorption efficiency of Cd^{2+} cations decreased in the second cycle with 35.27% and in the third cycle almost is constant.

7. Conclusions

The charcoal from wood branches activated with NaOH by hydrothermal method (BCBH) with 387.88 m^2/g surface area can explain the higher adsorption efficiency of MO (98.14 %) and (97.55 %) from mono respectively, di-solute aqueous solutions.

The best adsorbents for uptake the Cd^{2+} cations are BCBHD1 and BCBHD2 which evidenced the high BET surface (241.388 m^2/g and 128.405 m^2/g respective), and the highest crystalline (73.6 % and 90.9 % respectively). On these adsorbents the efficiency removal of Cd^{2+} cations are 69.62 %/BCBHD1 and 60.42 %/BCBHD2. The charcoal (BCBH) can be a good support for TiO_2 for to obtain the composites for adsorption of dye (MO) and heavy metals (Cd^{2+} cations), but a large amount of TiO_2 embedded into charcoal (BCBHD3) decrees the BET surface (74.267 m^2/g) and don't favor de adsorption of MO or of Cd^{2+} cations.

The adsorption efficiency of MO is increased in present of the Cd^{2+} cations, which are adsorbed in pores of the substrate and MO adsorption happen on the heterogeneous composite BCBH: TiO_2 surface. The kinetic studies showed that MO and Cd^{2+} cations adsorption process followed pseudo-second-order kinetics models ($R^2 > 0.94$ even 1). Langmuir and Freundlich equations both are applicable to describe the adsorption of MO on charcoal and composites within this initial dye concentration range. The constant value, R_L (low separation factor), in Langmuir isotherm and Freundlich constant, n, both give an indication of favourable adsorption.

The results show that the adsorption mechanism for removing MO and MO + Cd^{2+} cations from wastewater by means of the above presented composites BCBH, BCBHD1, BCBHD2, and BCBHD3 is a viable, low cost, up-scalable and sustainable for the adsorption technology.

Acknowledgements

References

Abdolali A., Ngo H.H., Guo W., Lu S., Chen S.S., Nguyen N.C., Zhang X., Wang J., Wu Y., (2016), A break through biosorbents in removing heavy metals: equilibrium, kinetic, thermodinamic and mechanism analyses in a lab-scale study, *Science of the Total Environment*, **542**, 603-611.

Alijeboree A.M., Alshirifi A.N., Alkaim A.F., (2017), Kinetics and equilibrium study for the adsorption of textile dyes on coconut shell activated carbon, *Arabian Journal of Chemistry*, **10**, 3381-3393.

Attara K., Bouazza D., Miloudi H., Tayeb A., Boos A., Sastre A.M., Demey H., (2018), Cadmium removal by a low-cost magadiite-based material: Characterization and sorption applications, *Journal of Environmental Chemical Engineering*, **6**, 5351-5360.

Bazrafshan E., Zarei A.A., Nadi H., Mohammad A.Z., (2014), Adsorptive removal of methyl Orange and Reactive Red 198 dyes by *Moringa peregrine* ash, *Indian Journal of Chemical Technology*, **21,** 105-113.

Bhatti H.N, Jabeen A., Iqbal M., Noreen S., Naseem Z., (2017), Adsorptive behavior of rice bran-based composites for malachite green dye: Isotherm, kinetic and thermodynamic studies, *Molecular Liquids*, **237**, 322-333.

Boamah P.O., Huang Y., Hua M., Zhang Q., Liu Y., Onumah J., Wang W., Song Y., (2015), Removal of cadmium from aqueous solution using low molecular weight chitosan derivative, *Carbohydrate Polymers*, **122**, 255-264.

Ciardelli G., Ranieri N., (2001), The treatment and reuse of wastewater in the textile industry by means of ozonation and electroflocculation, *Water Resources*, **35**, 567-572.

Chakraborty S., Chowdhury S., Saha P.D., (2011), Adsorption of Crystal Violet from aqueous solution onto NaOH-modified rice husk, *Carbohydrates Polymers*, **86**, 1533-1541.

Guerrero-Coronilla I., Aranda-Garcia E., Cristiani-Urbina E., (2019), Biosorption of metanil yellow dye from aqueous solutions by the entire water hyacinth plant (*Eichhornia crassipes*) and its vegetative organs, *Environmental Engineering and Management Journal,* **18**, 1671-1682.

Deshmukh P.D., Khadse G.K., Shinde V.S., Labhasetwar P., (2017), Cadmium removal from aqueous solutions using dried banana peels as an adsorbent: kinetics and equilibrium modeling, *Journal of Bioremediation & Biodegradation*, **8**, 395, doi: 10.4172/2155-6199.1000395.

Duman G., Onal Y., Okutucu C., Onenc S., Yanik J., (2009), Production of activated carbon from pine cone and evaluation of its physical chemical and adsorption properties, *Energy & Fuels*, **23**, 2197-2204.

Dutta A., Diao Y., Jain R., Rene E.R., Dutta S., (2015), Adsorption of cadmium from aqueous solutions onto coffee grounds and wheat straw: equilibrium and kinetic study, *Journal of Environmental Engineering,* **142,** 9.

El-Shafey E.I., Ali S.N.F., Al-Busafi S., Al-Lawati H.A.J., (2016), Preparation and characterization of surface functionalized activated carbons from date palm leaflets and application for methylene blue removal, *Journal of Environmental Chemical Engineering*, **4**, 2713-2724.

Gupta V.K., Nayak A., (2012), Cadmium removal and recovery from aqueous solutions by novel adsorbents prepared from orange peel and Fe_2O_3 nanoparticles, *Chemical Engineering Journal*, **180**, 81-90.

Hema M., Arivoli S., (2007), Comparative study on the adsorption kinetics and thermodinamics of dyes onto acid activated low cost carbon, *International Journal of Physical Science*, **2**, 010-017.

Ho Y.S., Mc-Kay G., (1998), The kinetic of sorption of basic dyes from aqueous solution by sphagnum Moss peat, *The Canadian Journal of Chemical Engineering*, **76**,

822-827.

Ho Y.S., Mc-Kay G., Wase D.A.J., Foster C.F., (2000), Study of the sorption of divalent metal ions on to peat, *Adsorption Science &. Technology*, **18**, 639-650.

Hsu L.J., Lee L.T., Lin C.C., (2011), Adsorption and photocatalytic degradation of polyvinyl alcohol in aqueous solution using P-25 TiO₂, *Chemical Engineering Journal*, **173**, 698-705.

Hydari S., Sharififard H., Nabavinia M., Parvizi M.R., (2012), A comparative investigation on removal performances of commercial activated carbon, chitosan biosorbent and chitosan/activated carbon composite for cadmium, *Chemical Engineering Journal*, **193-194**, 276-282.

Janusz W., Matysek M., (2006), Coadsorption of Cd (II) and oxalate ions at the TiO₂/electrolyte solution interface, *Journal of Colloid and Interface Science,* **296**, 22-29.

Kolodynska D., Halas P., Franus M., Hubicki Z., (2017), Zeolite properties improvement by chitosan modification - Sorption studies, *Journal of Industrial and Engineering Chemistry*, **52**, 187-196.

Kumar R., Ahmad R., (2011), Biosorption of hazardous crystal violet dye from aqueous solution onto treated ginger waste (TGW), *Desalination*, **265**, 112-118.

Mahmoud H.R, Ibrahim S.M., El-Molla S.A, (2016), Textile dye removal from aqueous solutions sing cheap MgO nanomaterials: Adsorption Kinetics studies and thermodynamics, *Advanced Powder Technology*, **27**, 223-231.

Mogaddasi F., Momen Heravi M., Bozorgmehr M.R., Ardalan P., Ardalan T., (2010), Kinetic and thermodynamic study on the removal of methyl orange from aqueous solution by adsorption onto camel thorn plant, *Asian Journal of Chemistry,* **22,** 5093-5100.

Li S., Lyons-Hart J., Banyasz J., Shafer K., (2001), Real-time evolved gas analysis by FTIR method: an experimental study of cellulose pyrolysis, *Fuel*, **80**, 1809-1817.

Liu Y., Sun X., Li B.U., (2010), Adsorption of Hg (II) and Cd (II) by ethylenediamine modified peanut shells, *Carbohydrate Polymers*, **81**, 335-339.

Mahmood T., Ali R., Naeem A.N., Hamayun M., Aslam M., (2017), Potential of used *Camellia sinensis* leaves as precursor for activated carbon preparation by chemical activation with H₃PO₄; optimization using response surface methodology, *Process Safety and Environmental Protection*, **109**, 548-563.

Matos J., Cuevas S.M., Ruiz-Delgado A., Oller I., Malato S., (2017), Development of TiO₂-C photocatalysts for solar treatment of polluted water, *Carbo*, **122**, 361-373.

Ofomaja A.E., Pholosi A., Naidoo E.B., (2015), Application of raw and modified pine biomass material for cesium removal from aqueous solutions, *Ecological Engineering*, **82**, 258-266.

Pattnaik P., Dangayach G.S., (2019), Sustainability of wastewater management in textile sectors: a conceptual framework, *Environmental Engineering and Management Journal,* **18**, 1947-1965.

Popa N., Visa M., (2017), The synthesis, activation and characterization of charcoal powder for the removal of methlene blue and cadmium from wastewater, *Advanced Powder Technology,* **28**, 1886-1876.

Pholosi A., Ofomaja A.E, Naidoo E.B., (2013), Effect of

chemical extract ants on the biosorptive properties of pine cone power: Influence on lead (II) removal mechanism, *Journal of Saudi Chemical Society*, **17**, 77-86.

Pyrznska K., (2019), Removal of cadmium from wastewaters with low-cost adsorbents, *Journal of Environmental Chemical Engineering*, **7**, 102795.

Robinson T., Chandran B., Nigam P., (2002), Effect of pretreatments of three waste residues, wheat straw, corncobs and barley husks on dye adsorption, *Bioresource Technology*, **85**, 119-124.

Sayğili H., Güzel F., Önal Y., (2015), Conversion of grape industrial processing waste to activated carbon sorbent and its performance in cationic and anionic dyes adsorption, *Cleaner Production,* **93**, 84-93.

Sewu D.D., Boakye P., Woo S.H., (2017), Highly efficient adsorption of cationic dye by biochar produced with Korean cabbage waste, *Bioresource Technology*, **224**, 206-213.

Sivaraj R., Namasivayam C., Kadirvelu K., (2001), Orange peel as an addorbent in the removal of acid violet 17 (acid dye) from aqueous solutions, *Waste Management*, **21**, 105-110.

Suhas G., Gupta V.K., Carrott P.J.M., Singh R., Chaudhary M., Kushwaha S., (2016), Cellulose: A review as natural, modified and activated carbon adsorbent, *Bioresource Technology,* **216**, 1066-1076.

Tseng R-L., Tseng S-K., (2005), Pore structure and adsorption performance of the KOH-activated carbons prepared from corncob, *Journal of Colloid and Interface Science,* **287**, 428-437.

Visa M., Duta A., (2008), Advanced Cd²⁺ removal on dispersed TiO₂ –fly ash, *Environmental Engineering and Management Journal,* **7**, 373-378.

Visa M., Nacu M., (2011), Comparative heavy metals and dyes removal efficiency on fly ash and wood ash, E*nvironmental Engineering and Management Journal,* **10**, 1407-1413.

Visa M., Andronic L., Lucaci D., Duta A., (2011), Concurrent dyes adsorption and photo-degradation on fly ash based substrates, *Adsorption Journal*, **17**, 102-108.

Visa M., Duta A., (2013), Methyl-orange and cadmium simultaneous removal using fly ash and photo-Fenton systems, *Journal of Hazardous Materials*, **244**, 773-779.

Yang C.L., Garrahan J.Mc, (2005), Electrochemical coagulation for textile effluent decolorization, *Journal of Hazardous Materials*, **B127**, 40-47.

Yang H., Yan R., Chen H., Lee D.H, Zheng C., (2007), Characteristics of hemicelluloses, cellulose and lignin pyrolysis, *Fuel*, **86,** 1781-1788.

Yagmur E, Tun M. S., Banford A., Aktas Z., (2013), Preparation of activated carbon from auto hydrolysed mixed southern hard wood, *Journal of Analytical and Applied Pyrolysis*, **104**, 470-478.

Zhang R., Zhang J., Zhang X., Dou C., Han R., (2014), Adsorption of Congo red from aqueous solutions using cationic surfactant modified wheat straw in batch mode: kinetic and equilibrium study, *Journal of the Taiwan Institute of Chemical Engineers,* **45**, 2578-2583.